Nanoscale Horizons

ROYAL SOCIETY OF CHEMISTRY

COMMUNICATION

View Article Online
View Journal | View Issue

Check for updates

Cite this: *Nanoscale Horiz.*, 2024, 9, 785

Received 29th January 2024,
Accepted 23rd February 2024

DOI: 10.1039/d4nh00041b

rsc.li/nanoscale-horizons

MoS_2 2D materials induce spinal cord neuroinflammation and neurotoxicity affecting locomotor performance in zebrafish†

Giuseppe Di Mauro,[a] Viviana Jehová González,[b] Francesco Bambini,[a]
Silvia Camarda,[a] Eduardo Prado,[c] Juan Pedro Holgado,[e] Ester Vázquez,[bd]
Laura Ballerini *[a] and Giada Cellot *[a]

MoS_2 nanosheets belong to an emerging family of nanomaterials named bidimensional transition metal dichalcogenides (2D TMDCs). The use of such promising materials, featuring outstanding chemical and physical properties, is expected to increase in several fields of science and technology, with an enhanced risk of environmental dispersion and associated wildlife and human exposures. In this framework, the assessment of MoS_2 nanosheets toxicity is instrumental to safe industrial developments. Currently, the impact of the nanomaterial on the nervous tissue is unexplored. In this work, we use as *in vivo* experimental model the early-stage zebrafish, to investigate whether mechano-chemically exfoliated MoS_2 nanosheets reach and affect, when added in the behavioral ambient, the nervous system. By high throughput screening of zebrafish larvae locomotor behavioral changes upon exposure to MoS_2 nanosheets and whole organism live imaging of spinal neuronal and glial cell calcium activity, we report that sub-acute and prolonged ambient exposures to MoS_2 nanosheets elicit locomotor abnormalities, dependent on dose and observation time. While 25 μg mL^{-1} concentration treatments exerted transient effects, 50 μg mL^{-1} ones induced long-lasting changes, correlated to neuroinflammation-driven alterations in the spinal cord, such as astrogliosis, glial intracellular calcium dysregulation, neuronal hyperactivity and motor axons retraction. By combining integrated technological approaches to zebrafish, we described that MoS_2 2D nanomaterials can reach, upon water (*i.e.* ambient) exposure, the nervous system of larvae, resulting in a direct neurological damage.

New concepts

Biomedical advances, including sensing devices, energy conversion or photoelectronic technologies, are increasingly based on new materials characterization and developments. In this framework, bidimensional transition metal dichalcogenides, including MoS_2 nanosheets, are at the core of research for industrial applications, with an expanding need to evaluate 2D nanosheets impact in the environment and in exposed humans. We investigated whether MoS_2 nanoflakes, upon ambient exposure, were internalized by organism to reach and affect the nervous system. To this aim, we used the larval zebrafish, an *in vivo* model organism suited to multi-technologies experimental design. We exploited high-throughput behavioral screening, allowing identification of MoS_2 neuro-toxic effects when delivered in the fish ambient, and we combined behavioral analysis with *in vivo* intracellular calcium imaging of nervous cells and with cryo-SEM/EDS. This multifaced approach provided mechanistic insights of the MoS_2 nanosheets cellular neuro-damage and internalization route. Our results show, for the first time, that upon ambient exposure MoS_2 may reach the zebrafish nervous system, resulting in a direct neurological damage. We put forward the hypothesis of MoS_2 internalization through the skin, thus the nanomaterial might reach, retrogradely *via* the skeletal muscles and the peripheral nervous system, the spinal cord igniting neuroinflammation-driven axons retraction, responsible for altered motor performance.

1. Introduction

2D TMDCs are a promising generation of nanomaterials which, due to their ultrathin structure coupled with favorable electronic and mechanical properties,[1] has attracted attention in diverse industrial and technological exploitations such as applications in energy conversion[2] or in photoelectronics[3] as well as frontier biodevices developments.[4] Among 2D TMDCs, MoS_2 is currently the most studied, thanks to its robustness and to the large availability in nature of the raw material.[5]

The broad applications of this nanomaterial will lead in the next years to augmented manufacturing of MoS_2 containing

---

[a] Neuron Physiology and Technology Lab, Neuroscience area, International School for Advanced Studies (SISSA), Via Bonomea 265, 34136, Trieste, Italy. E-mail: laura.ballerini@sissa.it, cellot@sissa.it

[b] Instituto Regional de Investigación Científica Aplicada (IRICA), UCLM, 13071 Ciudad Real, Spain

[c] Department of Applied Physics, Faculty of Science, University of Castilla La Mancha, Avda. Camilo José Cela 10, 13071 Ciudad Real, Spain

[d] Facultad de Ciencias y Tecnologías Químicas, UCLM, Avda. Camilo José Cela S/N, Ciudad Real, Spain

[e] Instituto de Ciencia de Materiales de Sevilla, Centro Mixto Universidad de Sevilla-CSIC, Américo Vespucio, 49, 41092 Sevilla, Spain

† Electronic supplementary information (ESI) available. See DOI: https://doi.org/10.1039/d4nh00041b

products, increasing risks of environmental dispersion,[6] potentially enhancing wildlife[7] and human exposures.[4] In addition, MoS_2 has been proposed as component of biomedical sensors, characterized by high levels of sophistication, hence directly interfaced to biological tissues.[8] Since following environmental or direct exposures, the nanomaterials may accumulate in the body and interact with tissues, possibly interfering with cell biology and causing hazardous effects,[9] the evaluation of MoS_2 nanomaterials biosafety is pivotal for their safe translation into use.

Although recent studies addressed MoS_2 nanosheets effects on different cell phenotypes and organs (reviewed in[4,10,11]), currently the impact of this nanomaterial on the nervous system remains unexplored.

Thanks to its feasibility for high throughput approaches,[12,13] combined with a physiological complexity similar to that of traditionally-used rodent models,[14] zebrafish has become a relevant *in vivo* paradigm for nanotoxicology studies.[15,16] Previous investigations have reported the use of zebrafish behavioral screening to assess the impact on the sensory motor nervous function of nanomaterials, including thermally reduced graphene oxide,[17] graphene quantum dots[18] and graphene oxide.[19]

In addition, due to its transparency, at the larval stage zebrafish is accessible for *in vivo* functional techniques, such as live imaging, which favors studies addressing the biological effects of nanomaterials/other toxicants on nervous system function with single cell resolution.[20–22]

In this work, we exploit the early-stage zebrafish to investigate whether mechano-chemically exfoliated MoS_2 nanosheets reach and affect, upon ambient exposure of the behaving larvae, the central nervous system.

We first addressed, by high throughput screening approaches, the emerging alterations in locomotor behavior when zebrafish are exposed to MoS_2, with these changes being reliable indicators of dysfunctions in the spinal cord network, the nervous structure deputed to locomotion control.[23] Our experiments showed that, the prolonged presence of MoS_2 nanosheets, at doses of 50 μg mL^{-1}, in the water ambient, induced a biphasic motor response, with a transient initial hyperactivity followed by a long-lasting depression in the fish swimming performance. By whole organism calcium imaging technique followed by immunostaining and microscopy, we documented that MoS_2 nanosheets progressively dysregulated glial calcium signaling, leading to astrogliosis and neuronal hyperactivity. These alterations were compatible with the emergence of neuroinflammatory reactivity due to the presence of MoS_2 in the spinal tissue, causing progressive degradation in the motor performance. Confocal microscopy and cryo-scanning electron microscopy (cryo-SEM) with energy dispersive spectroscopy (EDS) confirmed the presence of MoS_2 in the spinal tissue. We proposed several pathways which may allow ambient MoS_2 delivery to the nervous system, but we favor the hypothesis that the nanomaterial could reach the spinal cord retrogradely *via* the skeletal muscle, where we detected MoS_2. Once in direct contact with the nervous tissue, MoS_2 nanosheets triggered neuroinflammation, altering glial and neuronal cell functions, as revealed by the abnormal behavior. By combining high throughput approaches for the screening of behavioral alterations with the monitoring of single cell function in whole organism, our work has confirmed the use of zebrafish as a suitable model for assessing the biosafety of MoS_2 nanomaterials for the nervous system.

2. Results

2.1 Characterization of nanomaterials

Different techniques were used to characterize the exfoliated MoS_2. As reported in ESI,† Fig. S1A, high resolution transmission electron microscopy (HRTEM) allowed the observation of nanomaterial layers in E3 zebrafish medium (see methods), showing flakes with an average size of 222.36 ± 106.36 nm. The size distribution of these layers is reported in ESI,† Fig. S1B. We also analyzed the size distribution of flakes after 2 and 24 hours dispersion in E3 zebrafish medium (Fig. 1(A) and (B)), which were 212.43 ± 100.63 nm after 2 hours (Fig. 1(C)) and 205.72 ± 107.80 nm after 24 hours (Fig. 1(D)), indicating a consistent size of nanosheets over time.

Thermogravimetric analysis (TGA) of the exfoliated MoS_2 under a nitrogen atmosphere is displayed in ESI,† Fig. S1C. The TGA results exhibited a weight loss of 6.2%, indicating a low density of defects.[24]

The structural properties of the exfoliated MoS_2 were analyzed through Raman spectroscopy (ESI,† Fig. S1D). The Raman spectra revealed two principal bands, E^1_{2g} at 376.93 cm^{-1} and A_{1g} at 402.85 cm^{-1}. By analyzing the Raman data, it was possible to estimate the number of layers in the nanomaterial, showing an average of 3.[25]

UV-Vis absorption spectroscopy was used to assess the colloidal stability of two concentrations (50 and 25 μg mL^{-1}) of MoS_2 during 24 hours in E3 zebrafish medium. The exfoliated MoS_2 samples were evaluated at 612 nm (Fig. 1(E)), revealing an average sedimentation of 16.5% and 31.9% after 2 hours, and of 38.3% and 44.6% after 24 hours, at 50 and 25 μg mL^{-1} respectively. As control, we tested the colloidal stability of molybdate salt in distilled water and E3 medium at 25 μg mL^{-1} and 50 μg mL^{-1} (ESI,† Fig. S1E and F), that exhibited higher stability in both media, when compared to the nanomaterial.

X-ray photoelectron spectroscopy (XPS) analysis (Fig. 1(F)) was used to compare the surface composition of MoS_2, before (blue traces) and after 24 hours incubation in E3 medium (red traces), with that of Na_2MoO_4 (black traces), revealing peaks for Mo, S, Na, O, and adventitious carbon without contaminants. Mo 3d signals showed a doublet with peaks at approximately 232.5 eV (Mo $3d_{3/2}$) and 233.0 eV (Mo $3_{d5/2}$), consistent with MoS_2. Na_2MoO_4 shows a Mo $3_{d5/2}$ peak (232.5 ± 0.1 eV) consistent with this compound. O1s spectra depicted peaks at about 530.5 eV for Na_2MoO_4, similar to reported values, and a peak at 535.3 eV for Na KLL Auger transition. MoS_2, before and after incubation in E3 medium had O1s peaks around 532.7 eV,

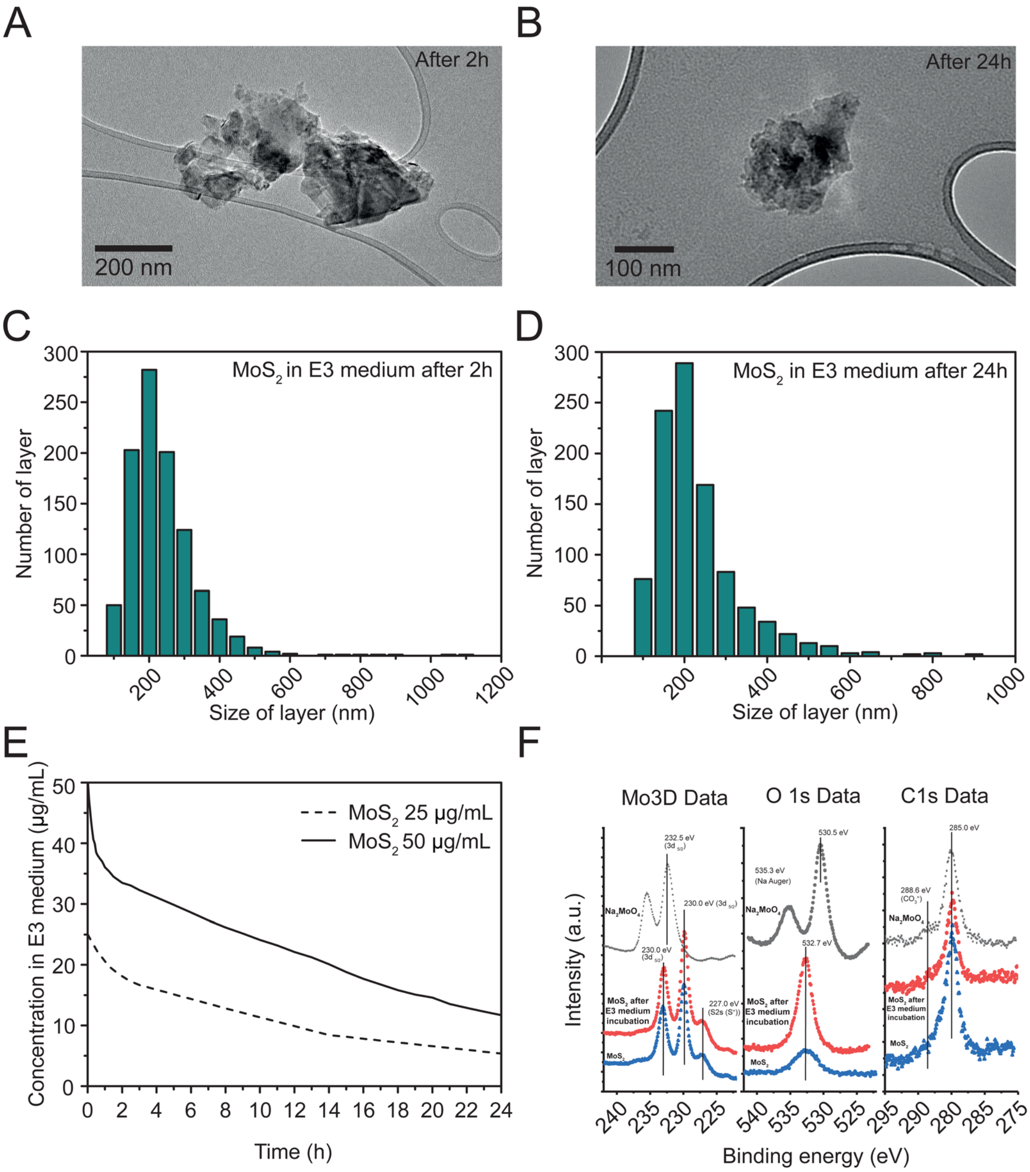

Fig. 1 Characterization of exfoliated MoS$_2$. (A) HRTEM images after 2 hours and (B) 24 hours and corresponding layer size distributions in E3 medium after 2 hours (C) and 24 hours (D). (E) Colloidal stability of MoS$_2$ in zebrafish E3 medium at 25 and 50 μg mL^{-1} during 24 h. (F) Signals from XPS analyses before (blue traces) and after 24 hours exposure to E3 medium (red traces). Molybdate salt (black traces) was used as reference control.

matching adsorbed $CO_{3=}$ species. After E3 incubation, MoS$_2$ showed much lower intensity for these species compared to the starting material. C1s signals, consistent across samples, had a main peak at about 285.0 eV and a shoulder at 288 eV, indicating low carbon concentration from atmospheric hydrocarbon species (CO$_2$ molecules) and absence of oxidized species on MoS$_2$, before and after E3 medium incubation.

2.2 MoS$_2$ nanoflakes alter locomotor behavior in zebrafish larvae

To investigate whether MoS$_2$ nanosheets interfere with the vertebrate sensory motor system, we dispersed the nanomaterial at two different sub-lethal concentrations (25 and 50 μg mL^{-1}, see ESI,† Fig. S2A and B) directly in the E3 medium (henceforth called also "water") of the zebrafish larvae and we performed behavioral, histological and single cell functional analyses after sub-acute (2 hours) and prolonged (24 hours) exposures (Fig. 2(A)). We used high throughput screening of locomotor behavior in response to light/dark cycles, a previously set paradigm enabling inter-individual comparative assessments of the sensory-motor responses.[17]

At 2 hours treatment by 25 μg mL^{-1} MoS$_2$ concentration, we measured an alteration in the swimming activity, resulting in a statistically significant ($P < 0.001$) increment in the distance moved during the dark phases (from 1092 ± 60 mm in control to 1785 ± 113 mm in MoS$_2$ treated larvae, Fig. 2(B)). Such an effect was transient and MoS$_2$ treated zebrafish recovered after 24 hours of incubation to a locomotor activity comparable to

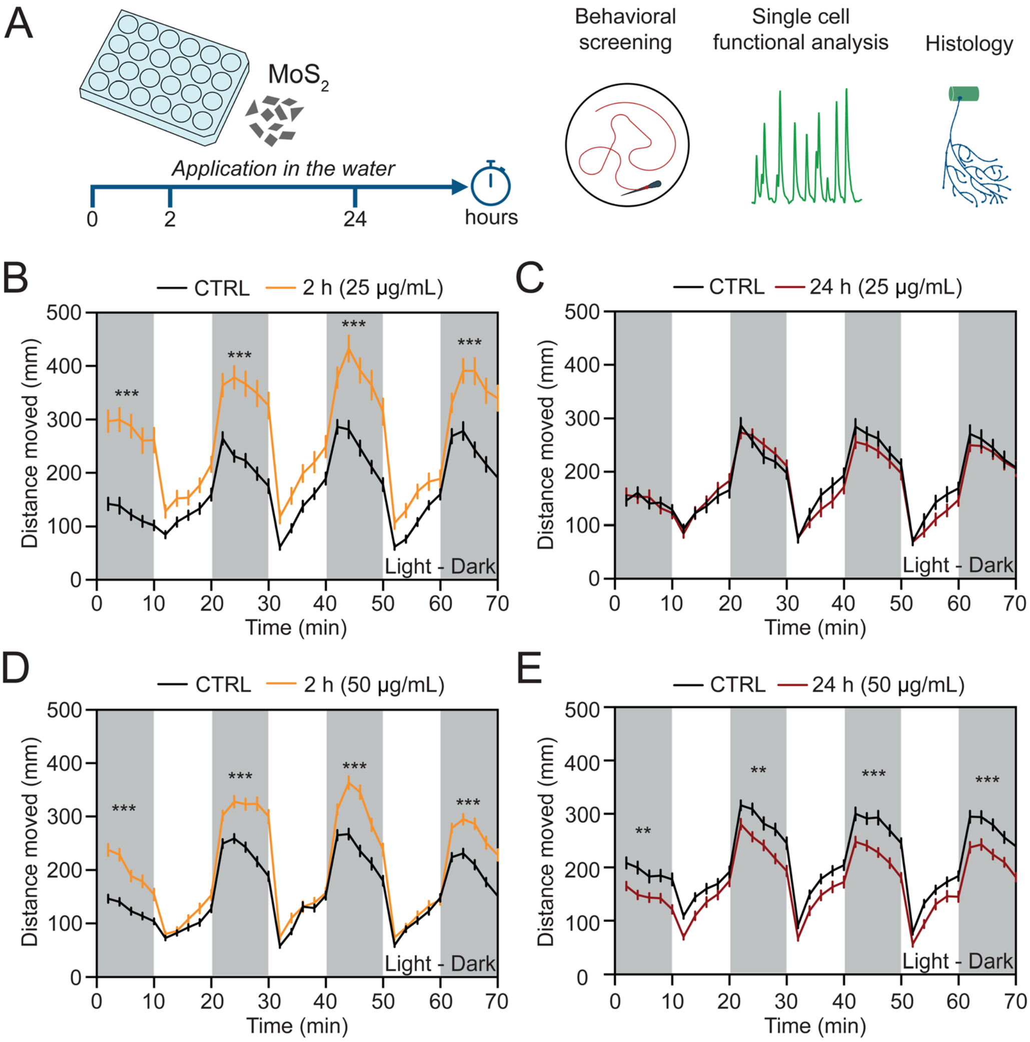

Fig. 2 Depending on the dose and the exposure time, MoS_2 nanosheets induce various alterations in zebrafish swimming performance. (A) Schematic representation of the experimental time line. MoS_2 nanosheets were dispersed in zebrafish water at two different concentrations (25 or 50 µg mL^{-1}) and their impact on the nervous system was evaluated after 2 or 24 hours (left) by using high throughput screening of locomotor activity, whole organism single cell calcium imaging and histological reconstruction (right). Locomotor performance was measured as distance moved during light and dark (white and grey bars, respectively) alternated periods (10 minutes each one). Line plots for the exposure to 25 µg mL^{-1} of concentration after 2 (B) and 24 hours (C) of treatment. Line plots for the exposure to 50 µg mL^{-1} of concentration after 2 (D) and 24 hours (E) of treatment. $N = 72$ larvae for each condition at the concentration of 25 µg mL^{-1} and $N = 96$ larvae for each condition at the concentration of 50 µg mL^{-1}. $^{**}P < 0.01$, $^{***}P < 0.001$.

unexposed control fish (1236 ± 55 mm and 1189 ± 60 mm of distance moved for control and MoS_2 treated larvae, respectively; $P > 0.05$, Fig. 2(C)).

When zebrafish were similarly treated, but with 50 µg mL^{-1} MoS_2 nanomaterial, after 2 hours the increase in swimming activity was also observed (from 1156 ± 43 mm of distance moved in control to 1576 ± 55 mm in MoS_2 treated larvae; $P < 0.001$, Fig. 2(D)). However, at this higher concentration, 24 hours long-lasting incubation induced persistent behavioral alterations, unexpectedly detected as a statistically significant decrease in the distance moved (from 1424 ± 53 mm in control to 1190 ± 46 mm in MoS_2 treated larvae; $P < 0.01$, Fig. 2(E)), namely a depression in locomotor activity. Additionally, the effects on locomotor behavior were specifically induced by MoS_2 nanosheets, since equimolar doses of molybdenum in the form of soluble molybdate did not alter swimming performance of treated zebrafish (ESI,† Fig. S3).

For both the MoS_2 concentrations tested, we analyzed after 24 hours the exposed larvae survival and anatomy. We visually detected deposition of MoS_2 aggregates on the surface of the zebrafish larvae (ESI,† Fig. S2A), with no changes in their survival rates (ESI,† Fig. S2B). Differently, the body size, measured as zebrafish length, height, and as yolk diameter (ESI,† Fig. S2C), was decreased in a statistically significant manner by the exposure to 50 µg mL^{-1} of MoS_2, but not at the lower concentration (ESI,† Fig. S2D–F).

All together, these experiments indicated that 25 µg mL^{-1} dose of MoS_2 produced a transient modification in the motor nervous function in zebrafish, with no effects on their gross anatomy. When we doubled the concentration, we induced long-lasting behavioral effects and the initial reactive hyperactivity was turned into a degradation of the locomotor performance, accompanied by morphological alterations.

2.3 Localization of MoS_2 nanoflakes in the spinal cord upon ambient exposure: confocal and ultra-microscopies

To ascertain whether the long-term downregulation of motor activity was due to MoS_2 (50 μg mL^{-1}) directly reaching and triggering reactive responses in spinal neuronal circuits, which control locomotion,[23] we explored MoS_2 nanosheets localization in the spinal cord after ambient E3 medium exposure. By confocal reflection microscopy in longitudinal spinal sections (Fig. 3(A)) of larvae exposed to MoS_2 (2 hours, 50 μg mL^{-1}), we detected reflection signals (red puncta in Fig. 3(B)) compatible with the presence of nanoflake aggregates within the spinal tissue. No reflection puncta were found in control zebrafish (Fig. 3(B)). Further analysis performed on the same spinal sections through cryo-SEM and EDS confirmed the nature of the aggregates as composed by MoS_2 (Fig. 3(C) and (D)). Molybdenum might be physiologically present in larvae tissues,[26] therefore, in our measures (Fig. 3(B)), to unambiguously report the presence of MoS_2 in the spinal cord of exposed zebrafish in respect to control (ESI,† Fig. S4A and B), we used EDS settings for molybdenum and sulfur to confirm the detection of nanomaterials.

Similarly, when analyzing the skeletal muscles innervated by the spinal system, through confocal reflection microscopy and cryo-SEM coupled to EDS, we detected the presence of MoS_2 nanosheets also in this tissue, but only when sampled from treated zebrafish (see ESI,† Fig. S5A and B). These tests suggest that MoS_2 nanosheets were internalized after their administration to the water, reaching the spinal nervous tissue.

2.4 Neuroinflammatory features in MoS_2 nanoflakes exposed zebrafish: spinal live calcium imaging and histology

In the next set of experiments, we investigated whether the nanomaterials, once localized in the spinal cord, ignited a neuroinflammatory response. Since altered calcium signaling in glial cells coupled to astrogliosis (*i.e.* increase in their size[27])

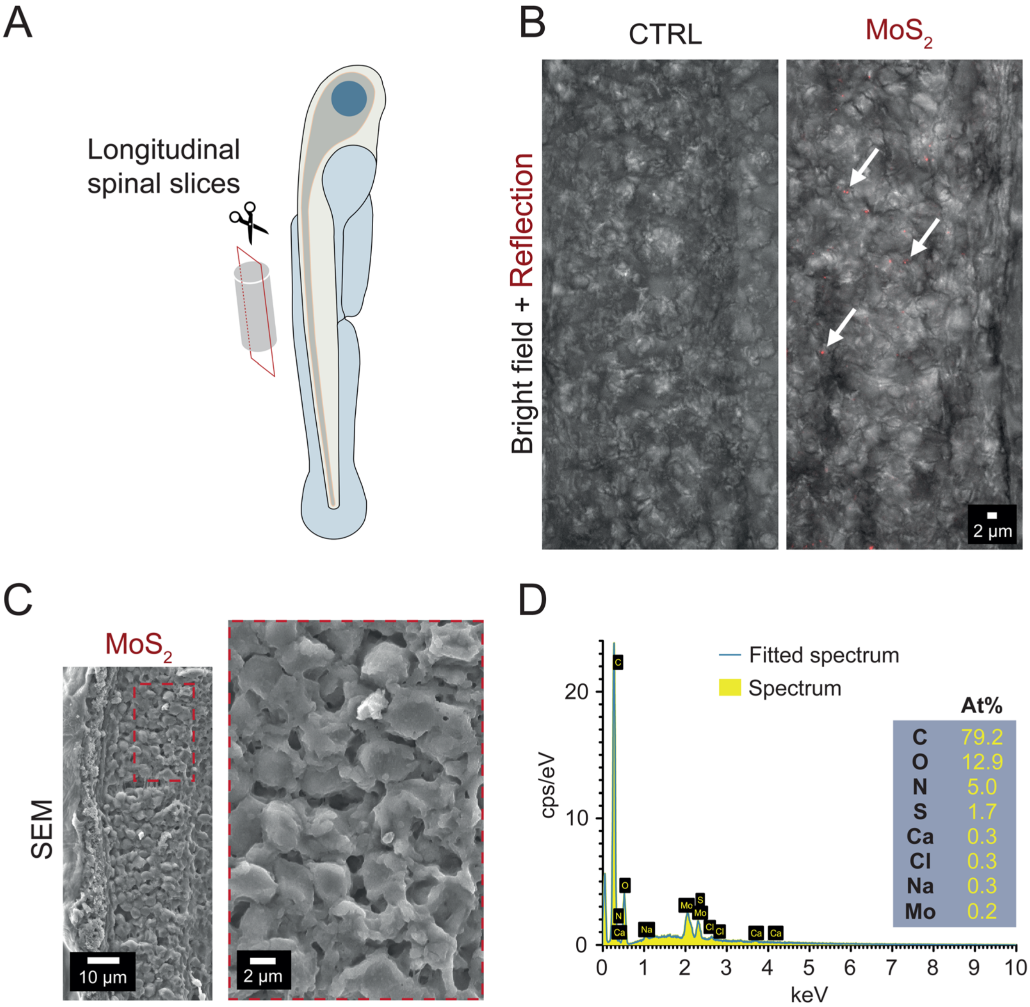

Fig. 3 After water administration, MoS_2 nanosheets are detected in the spinal cord of zebrafish. (A) Sketch of spinal cord slicing procedure to obtain longitudinal sections. (B) Z-stack reconstructions of the spinal cord of control (left) and MoS_2 exposed zebrafish (50 μg mL^{-1}, 2 hours; right). Images show an overlap of the bright field and reflection mode acquisitions. (C) SEM micrograph of the spinal cord obtained from larvae exposed to MoS_2 (50 μg mL^{-1}, 2 hours). The area in the dashed red rectangular in the left image is magnified in the right one. (D) Compositional analysis performed by EDS.

are hallmarks of neuroinflammation,[28–30] we investigated, in larvae exposed to MoS_2 nanoflakes, glial functionality and morphology through whole organism calcium imaging technique and immunohistochemistry. 2 or 24 hours after MoS_2 treatment (50 μg mL^{-1}), we micro-injected in the zebrafish spinal cord the calcium sensitive fluorescent dye Oregon Green™ 488 BAPTA-2, AM (0.1 μL at the concentration of 1 mM; see Methods) to monitor intracellular calcium dynamics.[31] After pharmacological silencing of neuronal firing and synaptic activity by tetrodotoxin (TTX, 1 μM) application, a blocker of the fast-inactivating voltage-gated sodium channels, we identified and measured in the spinal cord of untreated control larvae the emergence of slow and large intracellular calcium transients (see methods for their kinetic characterization), typically generated by glial cells[28,30] (Fig. 4(A)). When zebrafish larvae were exposed to the nanomaterial, the frequency of these slow calcium events was increased from 0.0055 ± 0.0004 Hz in control to 0.0075 ± 0.0009 Hz after 2 hours of MoS_2 treatment ($P > 0.05$, Fig. 4(B) and (C)), and further increased to 0.0137 ± 0.0014 Hz after 24 hours of incubation ($P < 0.001$, Fig. 4(B) and (C)).

Next, we immunolabelled spinal cords against glial fibrillary acidic protein (GFAP) a specific cytoskeletal marker for glial cells;[32] GFAP positive astrocytes in MoS_2 nanoflakes dysfunctional spinal cords were characterized by progressive astrogliosis, as expected in reactive glial cells. This phenomenon was quantified measuring their total volume (from 4380 ± 161 μm^3 in control to 4910 ± 169 μm^3 after 2 hours and 6957 ± 288 μm^3 after 24 hours of MoS_2; $P > 0.05$ and $P < 0.001$, respectively; Fig. 4(D) and (E)). These findings suggested that, *via* activation of glial cells, water applied MoS_2 nanoflakes induced cell reactivity and neuroinflammatory status in the spinal cord.

Neuroinflammation is reported to cause neuronal hyperactivity,[28,33] hence we evaluated by live imaging the presence of altered activity in spinal neurons. In standard saline solution, we monitored intracellular calcium transients (known to be activated by synchronized synaptic activity[34,35]) in neurons located in the ventral (motor) – spinal area. Calcium transients generated in neurons were identified pharmacologically, as they were completely abolished by TTX application, typically characterized by fast kinetics[29] (see methods for their kinetic characterization). When analyzing zebrafish exposed to MoS_2 nanoflakes (2 hours), we detected an enhancement in the frequency of neuronal calcium oscillations (from 0.0604 ± 0.0035 Hz in control to 0.0897 ± 0.0039 Hz after 2 hours MoS_2; $P < 0.001$; Fig. 4(F) and (G)), to an extent which correlated well with the boosting in locomotor behavior observed at this temporal point of the nanomaterial exposure. The frequency of neuronal calcium signals and thus of ventral circuit synchronized synaptic events, was further enhanced by prolonging the incubation up to 24 hours (0.1205 ± 0.0076 Hz; $P < 0.001$ control *vs.* 24 hours MoS_2; Fig. 4(F) and (G)), at this stage becoming unreflective of locomotor performance. In fact, the behavioral results showed a reduction in the swimming activity after 24 hours MoS_2 nanoflakes incubation.

Such a discrepancy between neuronal hyperactivity and locomotor function might depend on a deteriorated neurotransmission between motoneuron axon terminals and skeletal muscles. To explore this scenario, we used an antibody against the neuronal marker acetylated tubulin,[36] and, in whole mounted larvae we directly visualized the integrity of motoneuron axons emerging from the ventral spinal cord. While no differences were detected after 2 hours of MoS_2 exposure (16 ± 2 axonal branches in control and 15 ± 1 axonal branches at 2 hours of MoS_2 treatment; $P > 0.05$), prolonging the incubation to 24 hours significantly decreased the axonal branching of motoneurons (10 ± 2 axonal branches, $P < 0.05$, Fig. 4(H) and (I)) innervating the skeletal muscle.

In sum, our results supported the hypothesis that, upon ambient exposure to MoS_2 nanoflakes functional and morphological alterations involving both glial and neuronal cells were detected in the zebrafish spinal cord. The observed altered calcium signaling in GFAP-positive astrocytes, combined with astrogliosis, and neuronal hyperactivity are all hallmarks of active neuroinflammation that might be activated by the nanomaterial after its translocation from the water to the nervous tissue. Prolonged neuroinflammation might have affected the integrity of motor axons.[37]

2.5 Direct application of MoS_2 nanosheets to the spinal cord specifically recapitulates calcium dysregulation observed after nanomaterial water application

In order to support the hypothesis that the neuroinflammatory alterations observed in the zebrafish spine were due to MoS_2 nanoflakes reaching the nervous tissue, we tested if the direct delivery of the nanomaterial to the spinal cord could reproduce similar alterations. We injected in the spinal cord MoS_2 nanosheets (10 μg mL^{-1}, dispersed in Evans physiological solution, see methods) and we monitored glial and neuronal activity after 2 hours (Fig. 5(A)). MoS_2 nanoflakes injected in the spinal cord triggered an increment in the frequency of glial calcium events respect to controls (larvae injected with Evans physiological solution only). After 2 hours from the injection, calcium events frequency was increased from 0.0069 ± 0.0007 Hz in control to 0.0153 ± 0.0020 Hz in MoS_2 injected zebrafish ($P < 0.001$, Fig. 5(B) and (C)). Neuronal calcium oscillations were also enhanced in their frequency upon injection of MoS_2 nanoflakes in the spinal cord (from 0.0606 ± 0.0035 Hz in control to 0.1287 ± 0.0100 Hz in MoS_2 injected zebrafish; $P < 0.001$, Fig. 5(D) and (E)). These results suggested that 2 hours of direct exposure to the nanomaterial was sufficient to elicit reactive alterations in the central nervous system, mirroring those observed when the nanomaterial was applied *via* the ambient water.

We further tested if the modifications observed in the spinal cells were dependent on the exposure to MoS_2 nanoflakes or more generically to increased molybdenum concentration. We used as source of molybdenum the sodium molybdate (Na_2MoO_4) salt,[26] which was injected in the spinal cord at 15 μg mL^{-1} of concentration (equimolar to the previously used concentration of MoS_2, see methods). Differently from nanostructured MoS_2 flakes, Na_2MoO_4 did not alter calcium signaling in glial (0.0054 ± 0.0007 Hz in Na_2MoO_4 injected zebrafish; $P > 0.05$, Fig. 5(B) and (C)), and in neuronal cells (0.0508 ± 0.0033 Hz in Na_2MoO_4

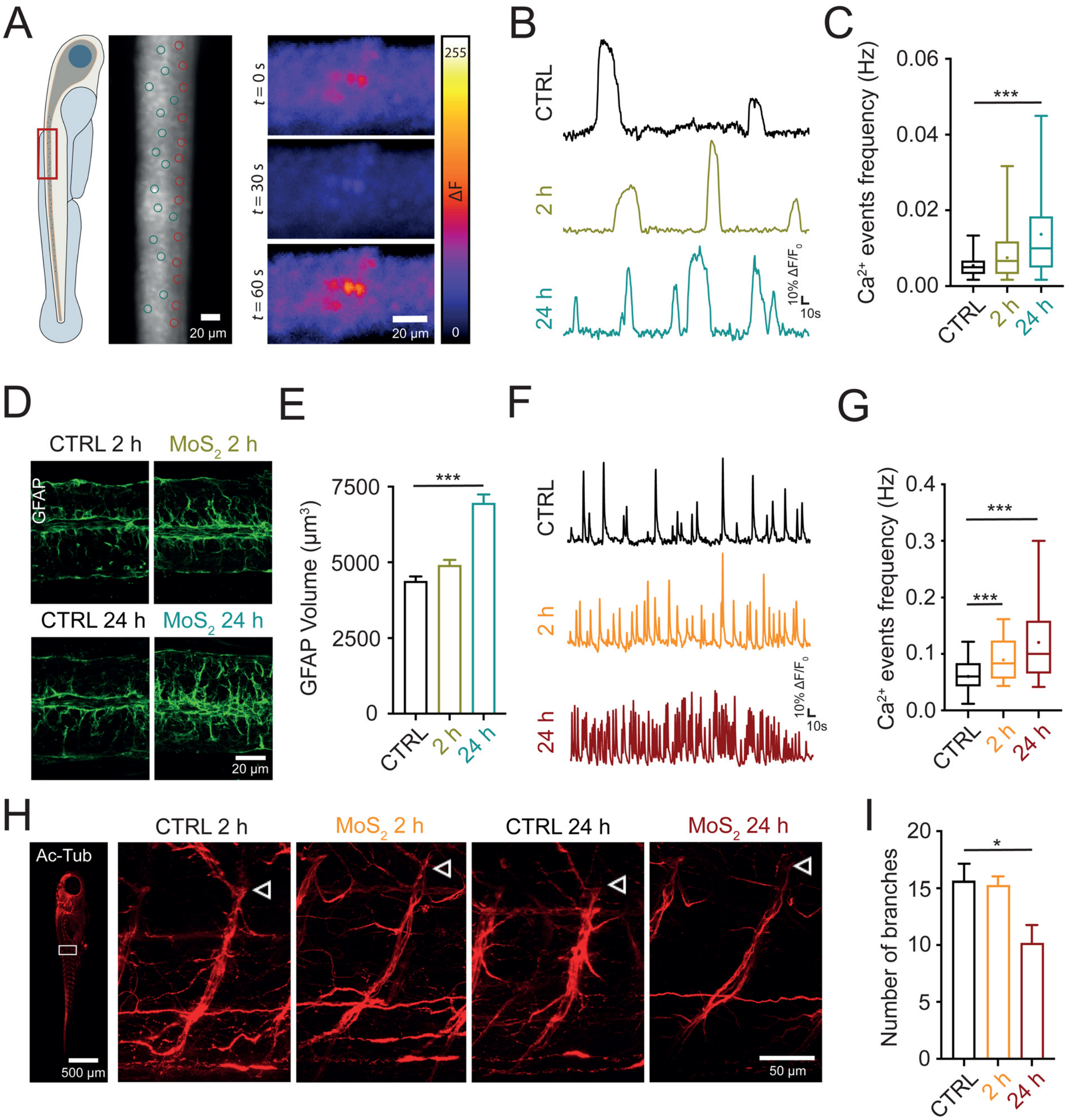

Fig. 4 Water applied MoS_2 nanosheets dysregulate calcium signaling in glial and neuronal cells of the spinal cord. (A) On the left, sketch showing that whole organism calcium imaging recordings were performed at the level of the spinal cord (red rectangle). In the middle, representative snapshot of a spinal cord portion during calcium imaging recording with exemplificative regions of interest (ROIs) used for the analysis of glial (green circle) and neuronal (red circle) cells. On the right, three temporally consecutive snapshots of a recording with fluorescence levels in false colors, showing the monitoring of intracellular calcium signaling at single cell level for glial cells. (B) Representative fluorescent traces of calcium oscillation activity from glial cells recorded in the different conditions. (C) Box plot of calcium events frequency for glial cells in control (*N* = 7 larvae, 43 cells), 2 hours MoS_2 (*N* = 8 larvae, 51 cells) and 24 hours MoS_2 (*N* = 10 larvae, 64 cells) treatments. Dots in the box plot correspond to the mean values. (D) Representative confocal images of longitudinal spinal slices immuno-stained for GFAP at 2 and 24 hours, for controls and MoS_2 treated larvae. Note that controls at 2 and 24 hours were similar and for this reason results were pooled together in the analysis. (E) Bar plot of quantitative analysis of GFAP volume in control (*N* = 27 larvae), 2 hours MoS_2 (*N* = 26 larvae) and 24 hours MoS_2 (*N* = 27 larvae) treatments. (F) Representative fluorescent traces of calcium oscillation activity from ventral spinal neurons recorded in the different conditions. (G) Box plot of calcium events frequency for neurons in control (*N* = 8 larvae, 58 cells), 2 hours MoS_2 (*N* = 10 larvae, 78 cells) and 24 hours MoS_2 (*N* = 13 larvae, 93 cells) treatments. Dots in the box plot correspond to the mean values. (H) Representative confocal images of whole mounted zebrafish immunostained for the acetylated tubulin. On the left an example of a whole larva, where the white rectangle indicates the area selected for analysis and magnified on the right for the different treatments at 2 and 24 hours. In these, white arrows indicate where the ventral root emerge from the spinal cord. To note, the decrease in branches of the ventral root formed by motoneuron axons after 24 hours MoS_2, controls at 2 and 24 hours were similar and for this reason were pooled together in the analysis. (I) Bar plot reporting the number of axonal branches in the ventral root of the spinal cord for control (*N* = 10 larvae), 2 hours MoS_2 (*N* = 10 larvae) and 24 hours MoS_2 (*N* = 12 larvae) treatments. *$P < 0.05$, ***$P < 0.001$.

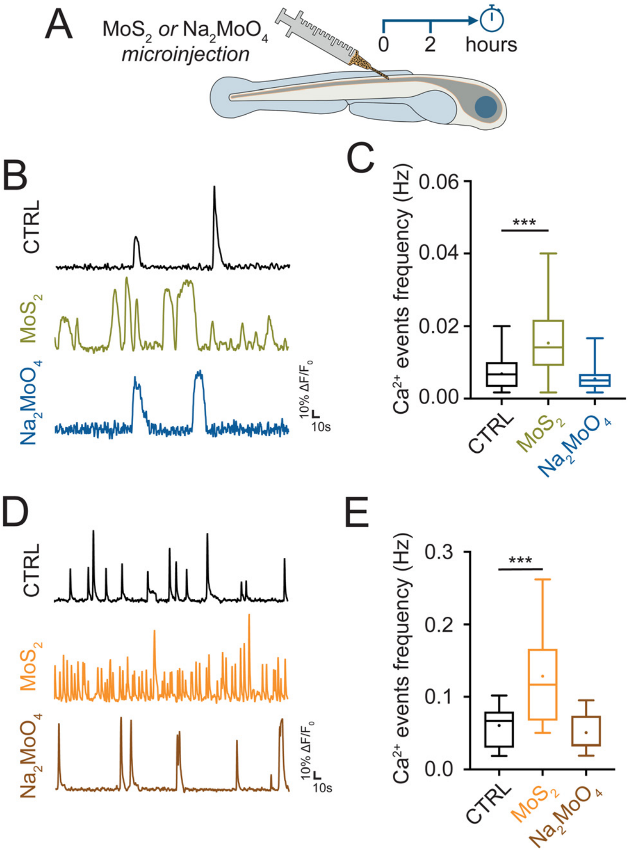

Fig. 5 Spinal injections of MoS_2 nanosheets alter glial and neuronal calcium signaling. (A) Schematic representation of the experimental time line. MoS_2 nanosheets or Na_2MoO_4 were directly injected in the spinal cord of zebrafish and their impact was evaluated after 2 hours (left) by whole organism calcium imaging technique. (B) Representative fluorescent traces of calcium oscillation activity from glial cells recorded in the different conditions. (C) Box plot of calcium events frequency for glial cells in control (N = 5 larvae, 42 cells), MoS_2 (N = 4 larvae, 20 cells) and Na_2MoO_4 (N = 4 larvae, 23 cells) treatments. Dots in the box plot correspond to the mean values. (D) Representative fluorescent traces of calcium oscillation activity from neurons recorded in the different conditions. (E) Box plot of calcium events frequency for ventral neurons in control (N = 7 larvae, 49 cells), MoS_2 (N = 6 larvae, 44 cells) and Na_2MoO_4 (N = 7 larvae, 59 cells) treatments. Dots in the box plot correspond to the mean values. ***$P < 0.001$.

injected zebrafish; $P > 0.05$, Fig. 5(D) and (E)). This experiment consistently supported the idea that the neuroinflammation was a response to the MoS_2 nanosheets rather than to the molybdenum *per se*.

3. Discussion

We report here that, when present in the ambient water, MoS_2 nanosheets induced in zebrafish locomotor alterations whose persistence was dose dependent, consistent with the nervous tissue reactivity to the translocation of the material to the spinal cord. Further exploring 50 μg mL^{-1} doses exposure suggested that such behavioral changes were associated with functional and histological hallmarks of neuroinflammation, such as glial dysfunctional calcium signaling and neuronal synaptic hyperactivity in the spinal cord, an area where, when examined by different microscopy approaches, the nanomaterials could be detected after ambient administration.

The two tested concentrations of MoS_2 (25 and 50 μg mL^{-1}), matched the range of those typically used for nanotoxicology studies in zebrafish,[38,39] yet being sub-lethal, as shown by the evaluation of the LD_{50} in our study. Notably, similar concentrations of molybdenum (in the form of molybdate) were reported to be not hazardous for freshwater organisms.[40]

25 μg mL^{-1} of MoS_2 treatment reversibly induced locomotor hyperactivity, which normalized upon 24 hours treatment. This transient effect might be related to the fast decrease of the dispersed nanomaterial concentration in water, due to precipitation, allowing only a small fraction of nanomaterial to enter the body and reach the spinal cord, with no progressive accumulation in the following 24 hours exposure. The reversibility of this initial reactivity might be due to the progressive degradation/clearance of the material from the biological environment[41] when MoS_2 was delivered at 25 μg mL^{-1} of concentration. We focused our mechanistic experiments on the higher dose, due to the persistence of motor abnormalities in these conditions. Incubations at 50 μg mL^{-1} of concentration, after an initial increase in swimming activity, which matches the direct observation of the nanomaterial in the spinal cord, resulted in the long-lasting degradation of locomotor performance, indicating that, probably due to inefficient clearance of higher doses, the materials triggered prolonged dysfunction.

Spinal cord calcium imaging displayed recordings at cellular resolution in intact paralyzed zebrafish[31] with signals generated by glial or neuronal cells, distinguished based on the sensitivity to TTX removal of action potentials[42] and on the different kinetic properties of the calcium oscillations.[29]

Thanks to this approach, we detected upon ambient administration of MoS_2 nanosheets, alterations in glial calcium signaling, with a progressive enhancement in cytoplasmatic calcium oscillation frequency, emerging already at 2 hours. Calcium oscillations are crucial intercellular communication signals within glial networks and reactive astrocytes typically display dysregulated calcium signaling in response to potential threats or injuring conditions.[43] When analyzing structurally GFAP-positive cells, we measured an increment in their volume, namely astrogliosis,[27] that, together with the intracellular calcium dysregulation, has been associated to neuroinflammation and reactive glial cells.[29,30] Activated astrocytes are aimed to protect the CNS integrity by removing the source of damage and promoting tissue repair.[44] However, when sustained, neuroinflammatory reactive glia can be detrimental, leading to neurodegeneration.[45] Another described feature of neuroinflammation is the hyperexcitability of the spinal neuronal network.[28,30,33] In our experiments, this was measured in treated fish as an enhancement in the frequency of neuronal calcium oscillations, driven by hyperactivity of spinal circuits.[46] Thus, all together our findings indicate that the water administration of MoS_2 nanosheets activate spinal cord reactivity with, in the absence of material clearance, typical neuroinflammation exacerbating loops.[47]

Spinal neuron network, *via* activation of motoneurons innervating skeletal muscles, governs locomotor activity,[48] thus the enhanced neuronal calcium signaling measured after 2 hours of MoS_2 treatment, reporting the increased neuronal synaptic activity,[46] might explain the locomotor hyperfunction monitored at such time point, with intact motoneuronal axonal branching. At 24 hours post-treatment, while neuroinflammation was further spreading (gliosis with glia enhanced calcium signaling), despite neuronal TTX-sensitive over activity, a deteriorated locomotor performance and a reduced axonal branching, indicative of axonal retraction,[49] were detected. We suggest that, prolonged neuroinflammation due to persistent MoS_2 presence in the spinal cord, induced secondary axonal damage and retraction in motoneurons[33] which resulted into a decrease in locomotor efficacy. We cannot exclude that the developmental delay found in MoS_2 exposed larvae, measured as reduction in their body size, also contributed to this phenomenon.

Our findings, that direct injection into the spinal cord of MoS_2 nanosheets elicited the same pattern of aberrant calcium signaling as in water exposed zebrafish, strengthen the hypothesis that the presence of the material in the nervous tissue triggers the irritative focus, when not cleared, and reactive glia. These effects were strictly induced by the nanostructured MoS_2 and did not arise as consequence of an unspecific increment of molybdenum in the tissue, in fact injections of molybdenum salts[26] did not alter calcium signaling.

These results, together with confocal reflection microscopy and cryo-SEM-EDS analysis, confirming the presence of the nanosheets in the spinal cord after water administration, supported the hypothesis that after ambient application the nanomaterial was internalized by the larvae and reached the spinal cord. It is tempting to speculate that nanostructured MoS_2 triggers neuroinflammation directly in the spinal system, although we cannot discard the hypothesis that, similarly to dispersible MoS_2 micro-sheets,[50] after entering the zebrafish organism the materials trigger pro-inflammatory responses in other organs[50] which then promote a secondary damage in the CNS.

Several pathways can be hypothesized for MoS_2 internalization. It has been reported that nanosheets with similar size to those used in our study, when water applied, crossed adult zebrafish epithelial barrier of different mucosae (nasal, gills, gut and skin).[51] In our experiments, we can however rule out the digestive system as the main source of internalization, since at the developmental stage used most zebrafish do not feed autonomously.[52] Alternatively, MoS_2 nanosheets might be internalized through the olfactory system, already mature at this early developmental stage,[53] and directly connected *via* olfactory sensory neurons to the central nervous system. Another internalization route could be the respiratory system, from where, as previously observed for other nanomaterials,[54] nanosheets would translocate first to the bloodstream circulation and by crossing the blood brain barrier would reach the nervous tissue. In agreement with this hypothesis, a previous work reported detection of MoS_2 nanosheets in zebrafish blood after their water application.[55] Further investigations will be required to explore these hypotheses, nevertheless our experimental evidence of altered locomotor behavior, spinal reactivity, motor axons damage combined to the presence of the material in the spinal system and in the skeletal muscle, support the hypothesis of an internalization route where MoS_2 nanosheets penetrate *via* the skin and skeletal muscles to be possibly retro-translocated to the spinal cord.

4. Conclusions

2D TMDCs are an emerging family of nanomaterials, whose use in several fields is expected to increase in the next years. However, a complete assessment of their biosafety is still lacking. By combining high throughput screening of locomotor behavior in zebrafish larvae exposed to MoS_2 nanosheets with whole organism calcium imaging to monitor spinal cell function, our work contributes to shedding light on the interaction of this nanomaterial with the function of the nervous system. We reported that ambient exposure to MoS_2 nanosheets elicited a variety of locomotor abnormalities, dependent on the used dose and observation time. While 25 $\mu g\ mL^{-1}$ concentration treatments exerted transient effects, 50 $\mu g\ mL^{-1}$ ones induced long-lasting modifications, strongly correlated to neuroinflammation driven alterations of the spinal cord, such as astrogliosis, glial intracellular calcium dysregulation and neuronal hyperactivity. We concluded that upon ambient exposure MoS_2 nanomaterials can reach the spinal cord, where they induce neurological damage. Future investigations, such as assessing the impact of MoS_2 lateral size on neurotoxicity and characterizing their long-term effects upon repeated chronic exposures, will be required for a complete evaluation of the risks associated to the use of this nanomaterial.

5. Methods

5.1 Synthesis and characterization of MoS_2 nanomaterial

The MoS_2 used in this study was obtained from Biograph Solutions, and its properties were previously compared with those of other commercially available nanomaterials as reported in.[56] MS_2 in bulk as the starting material and glycine as the exfoliating agent were both sourced from Sigma-Aldrich. For the synthesis of exfoliated MoS_2, we followed the methodology described in.[24] The procedure involved the use of 75 mg of bulk MoS_2 and 2.5 g of glycine. These materials were placed in a 250 mL stainless steel jar containing 15 stainless steel balls with a diameter of 2 cm. The ball-milling process was carried out using a Retsch pm100 machine.

After the milling process, the resulting powder was dispersed in 100 mL of water to remove the glycine present in the media through dialysis. The dispersion underwent five consecutive water washes, with each wash performed every 90 minutes (including an overnight change). Finally, the solutions were subjected to lyophilization at −80 °C under a pressure of 0.005 bar to obtain powdered samples of exfoliated MoS_2.

5.2 Transmission electron microscopy (TEM)

TEM analyses were conducted on stable dispersions of the nanomaterial, at 0, 2 and 24 h of incubation in E3 medium, after appropriated dilution. The diluted samples were then dip-casted onto Lacey copper grids (3.00 mm, 200 mesh) that were coated with a carbon film and subsequently dried under vacuum conditions. The investigations were carried out using a HRTEM model JEOL 2100, operating at an accelerating voltage of 100 kV. 1000 flakes were analyzed for each temporal point.

5.3 Thermal gravimetric analysis (TGA)

TGA was conducted using a TA Instruments Q50 apparatus with a heating rate of 10 °C per minute under either a nitrogen or air atmosphere, depending on the nature of the sample, within the temperature range of 100 to 900 °C.

5.4 Raman spectroscopy

Raman spectra were obtained using an InVia Renishaw microspectrometer, which was equipped with a 532 nm laser focused at a single point. To prevent laser-induced heating effects, the power density was maintained below 1 mW μm^2 in all experiments. The Raman analyses were conducted on solid-state samples under normal environmental conditions. The resulting spectra were acquired by randomly selecting and analyzing at least 30–40 different locations on each sample. This analysis revealed that the MoS_2 used in this study was 2H phase, a feature relevant in the use of nanomaterials as previously reported in.[57]

5.5 Stability of MoS_2 in the zebrafish E3 medium

UV spectroscopy was employed to measure nanomaterial stability in zebrafish E3 medium using a UV-Vis Cary 5000 UV-vis-NIR spectrophotometer with 1 cm quartz cuvettes. E3 medium (for simplicity also named water in the results), was composed as follows (in mM): 5 NaCl, 0.17 KCl, 0.33 $CaCl_2$, 0.33 $MgSO_4$.

The scans of the samples were recorded at 612 nm for MoS_2 for 24 hours at different concentrations (25 and 50 $\mu g\ mL^{-1}$). The concentration of the samples was determined using the Lambert–Beer law, according to the calibration curve shown in ESI,† Fig. S6 and Table S1.

5.6 X-ray photoelectron spectroscopy (XPS)

XPS analyses were carried out by using a SPECS Phoibos 150 instrument using a non-monochromatic Al K alpha X-ray source (20 mA, 14 kV). The instrument BE energy scale (work function) was calibrated to give a binding energy (BE) at 83.96 eV for the Au 4f7/2 signal for freshly ion etched metallic gold (Au). The spectrometer dispersion (energy range) was adjusted to give a BE at 932.62 eV for the Cu 2p3/2 line of freshly ion etched metallic copper (Cu). The charge compensation (neutralizer) system was used on all non-conductive specimen samples. The surface of each non-conductive sample was irradiated with a flood of electrons accelerated to 2.0–4.0 eV to produce a nearly neutral surface charge. Survey scan analyses (0–1100 eV range) were carried out by using a pass energy of 50 eV. High energy resolution chemical state analyses (20–50 eV wide range) were carried out by using a pass energy of 20 eV. Data from all insulating materials have been charge corrected (referenced) using the main signal of the carbon 1s spectrum (hydrocarbon, C–C, moiety) assigned to occur at 284.6 eV. In fact, the calibration of the binding energy has been based on an interactive assignment where gold was deposited by sputtering onto the pellet of sodium molybdate. The $Au4f_{7/2}$ gold was assigned a value of 84.0 eV, resulting on a value of 284.5 ± 0.1 eV for main C1s peak, a value that could be assigned on graphitic species coming from adventitious carbon from atmospheric species adsorption onto the sample during preparation onto the sample holder.

5.7 Zebrafish treatments

Zebrafish (*Danio rerio*) embryos were provided by the University of Trieste (Italy), while all the experiments were performed at the International School for Advanced Studies (SISSA, Italy). Zebrafish were used in accordance with the Italian law (decree 26/14) and the EU guidelines (2007/526/CE and 2010/63/UE). Experimental activities were approved by the authority veterinary service and by our institution (SISSA) animal wellbeing committee (OBPA).

Zebrafish were maintained in E3 medium at the temperature of 28.5 °C and in a light : dark cycle of 12 : 12 hours until the age of 5 days post fertilization (dpf), when zebrafish were used for experiments.

The nanomaterial was dispersed in the E3 zebrafish medium at the concentrations of 25 and 50 $\mu g\ mL^{-1}$. To ensure the homogenous of dispersion, the solution was sonicated for 20 minutes in the sonicator bath (J.P. Selecta – Ultrasons, H-D). Larvae were exposed to the dispersed nanomaterials starting at the age of 5 dpf or at the age of 4 dpf and they were analyzed through behavioral experiments, calcium imaging recordings and histological characterization after 2 and 24 hours, respectively. All behavioral experiments, calcium imaging recordings and histological characterizations were performed at 5 dpf.

In calcium imaging experiments in which the nanomaterial was intra-spinally injected, the MoS_2 concentration was 10 $\mu g\ mL^{-1}$, solved in Evans physiological solution, whose composition was (in mM): 134 NaCl, 2.9 KCl, 2.1 $CaCl_2$, 1.2 $MgCl_2$, 10 Glucose, 10 HEPES, pH 7.8. A volume of 0.1 μL of solution was injected in each fish. Such lower concentration was in the range of those used in previous works where nervous tissue was directly exposed to nanomaterials.[30,58,59] Control larvae were injected with the same volume of Evans physiological solution deprived of nanomaterials.

In a parallel set of larvae, Na_2MoO_4 salt (Sigma-Aldrich) was injected. This was diluted in Evans physiological solution at a concentration of 15 $\mu g\ ml^{-1}$, in order to have an equimolar concentration of Mo respect to that in MoS_2.

5.8 Behavioral experiments

High-throughput screening of locomotor behavior was performed using the light–dark assay, commonly used to evaluate the function of the sensory-motor nervous system.[17,60] The apparatus was composed by a recording chamber with an Infra-Red (IR) backlight unit interfaced with a monochrome IR sensitive camera GigE (Blaser, 60 frames per second) and equipped with a light–dark module to allow the stimulation and temperature control of 27 °C.[17] Larvae were introduced in the recording chamber inside a 24-multiwell plate system (one animal for each well) and habituated for 15 minutes. Larvae were then exposed to 3 consecutive cycles of 10 minutes alternated light–dark periods while their locomotor activity was video-recorded. The EthoVision XT (Noldus, Netherlands) software was used to track animal movements, allowing to calculate the distance moved (mm) as the total distance that the larvae traveled during the considered interval time. For each experimental condition, we tested three separate biological replicates. Data were reported in line plots (Fig. 2) as averaged distance moved in bin of 2 minutes time, while statistics was performed on the entire 10 minutes periods of light or dark. To avoid redundancies, in the results we reported behavioral data as Mean ± S.E.M. and *P*-values related to the first light–dark transition only, although results were congruent also in the following light–dark transitions as shown in Fig. 2.

5.9 Analysis of survival and anatomical traits

After 24 hours of incubation, we assessed the impact of MoS_2 nanosheets (25 and 50 μg mL^{-1}) on zebrafish survival and anatomical development. For the first parameter, larvae were considered alive when detecting heartbeat. For the analysis of anatomical traits, larvae were anesthetized with 0.02% of MS222[61] (Sigma) and fixed overnight in 4% paraformaldehyde (PFA, solved in phosphate buffered saline, PBS) at 4 °C. Next, the samples were washed in PBS and mounted on glass microscope slides. The images were acquired using EVOS XL Core Imaging System with 4× objective and analyzed using Fiji software. In order to evaluate the developmental stage, we considered the following anatomical traits: standard length (SL) as the distance from caudal peduncle to snout, height at anterior of anal fin (HAA), yolk diameter as the distance at the shorter axis.[22,62]

5.10 Confocal reflection microscopy

The light reflection properties of MoS_2 were exploited to identify the tissue localization of the nanomaterial after its administration in the water. After assessing that the nanomaterial dispersed in E3 solution could reflect light of 636 nm wavelength, we applied this approach to longitudinal sections of spinal cord. For their preparation, after the treatment with the nanomaterial, larvae were fixed with 4% PFA overnight at 4 °C and preserved in 20% sucrose in PBS overnight at 4 °C. After several washes in PBS, they were embedded in killik (OTC compound, BioOptica) and sliced longitudinally using the cryostat (OTF5000, BioOptica) at the thickness of 30 μm. Samples of nanomaterial treated and untreated larvae were acquired at the confocal microscope at the magnification of 100× (oil objective, NA = 1.45) using a 0.5 μm step through the entire thickness of the larvae and then analyzed using the Fiji software.

5.11 Cryo-scanning electron microscopy (SEM) and energy dispersive spectroscopy (EDS)

We conducted SEM imaging, elemental mapping, and EDS analyses using the GeminiSEM 500 field emission instrument from Zeiss. The surface composition was quantitatively determined by employing EDS with an 80 mm^2 detector from Oxford, UK, specifically to measure the concentration of Mo and S in the samples. To observe and capture images, we utilized cryo-SEM (Model: PP3010 Quorum, UK) equipped with a field emission scanning electron microscope (Zeiss GeminiSEM 500, Oberkochen, Germany) in high vacuum mode. The imaging process involved using an accelerating voltage of 2 kV and applying a metallic coating. To analyze the composition in specific areas, we performed small-scale compositional analyses to compare the control samples with those exposed to MoS_2.

5.12 Whole organism calcium imaging technique

For calcium imaging experiments, during their development larvae were maintained in E3 solution containing 0.003% of *N*-phenyltiourea (PTU), to reduce melanin formation and increase larva transparency.[63]

To record intracellular calcium oscillations in the cells of the spinal nervous system, we used the calcium sensitive dye Oregon Green 488 BAPTA-1, AM (Thermofisher). The dye was solved in Pluronic F-127 20% solution in DMSO (Thermofisher) to generate a 10 mM stock solution. This was diluted in filtered Evans solution at the final concentration of 1 mM.[31] Zebrafish larvae were placed in Evans physiological solution, anesthetized in 0.02% of MS222 and pinned on their side into a Sylgard-coated imaging chamber by pressing short pieces of fine tungsten wire through the notochord.[22] Intra-spinal injections of the calcium sensitive dye containing solution were obtained by using a fine glass pipette (tip diameter ∼5 um), under the control of a micromanipulator (WR-88, Narishige). The pipette was gently inserted first in the larva body at level of the 9th–10th somites and then in the spinal cord. Solutions were delivered through pressure pulses through a microinjector (PDES-02DX; 20 puffs of 150 ms at a pressure of 1.5 bars), corresponding to an injected volume of 0.1 μL. When MoS_2 or Na_2MoO_4 were injected in the spinal cord, they were administered in the same solution containing the calcium sensitive dye.

Calcium imaging recordings were acquired by means of a Hamamatsu digital camera (C11440-22CU Orca-flash4.0) mounted on a Nikon Eclipse Ti-U inverted microscope and controlled by the HCIimage software. Each animal was recorded for 10 minutes while continuously perfused with Evans physiological solution supplied with tubocurarine (10 μM, Sigma, to prevent skeletal muscle contractions) with a flow rate of 3 mL per minute. A mercury lamp (Nikon intensilight C-HGFI; ND = 4) provided the excitation light (488 nm) to stimulate the calcium sensitive dye, emitting the fluorescent signal subsequently filtered by a 395 dichroic mirror and captured by the camera. All images were acquired with a 40× (0.6 NA) objective, resolution of 512 × 512, binning 4 × 4 and exposure time of 150 ms.

Next, larvae were recorded for further 10 minutes while applying in Evans physiological solution tubocurarine (10 μM) and tetrodotoxin (TTX, 2 μM, HelloBio) to isolate calcium signals from glial cells.[18]

Recordings were analyzed with FiJi ImageJ software selecting 10 ± 5 cells ROIs for each spinal cord. Related traces were transferred to Clampfit software (10.6 version; Molecular Device LLC, US) and calcium transients were expressed as $\Delta F/F_0$, where ΔF corresponds to the fluorescence rise over the baseline F_0.

Calcium oscillations generated by neurons could be distinguished from glial ones, as they were abolished by TTX[29] (see ESI,† Fig. S7) and for their different kinetics. Neuronal calcium oscillations presented shorter duration (5.4 ± 0.5 s) and faster frequency (0.06 ± 0.003 Hz) respect to those generated in glial cells (21.8 ± 2 s and 0.005 ± 0.0008 Hz, values calculated in N = 10 cells of control), as reported in literature.[29]

In an additional set of experiments (see ESI,† Fig. S8), MoS_2 nanosheets were injected at a lower concentration (5 μg mL^{-1}), inducing alterations only in neuronal signaling but not in the glial one.

5.13 Immunofluorescence reconstruction of spinal nervous system

Whole mount immunofluorescence of spinal tissue was carried out as in[17] with some modifications. Zebrafish larvae were anesthetized with 0.02% of MS222 in E3 medium and fixed using 4% PFA in PBS overnight at 4 °C. The day after, the larvae were washed with PBS and depigmented for 40 minutes in in Milli-Q water containing H_2O_2 (3%) and KOH (1%) at room temperature (RT). After PBS washes, larvae were quenched for 30 minutes in glycine (0.1 M, Sigma-Aldrich) and washed again in PBS. In order to increase permeability of membrane and the probability of the antibody to reach the antigen, larvae were exposed to absolute acetone for 7 minutes at −20 °C, then washed in PBS and treated with collagenase (2 mg mL^{-1}, Sigma-Aldrich) for 40 minutes at RT. After PBS washes, larvae were first incubated for 2 hours at RT in the immuno-blocking solution (IB, 4% normal goat serum, NGS, 1% DMSO, 0.8% Triton X-100 in PBS) to block the nonspecific sites, and later for 72 hours at 4 °C in IB with the primary mouse antibody against the acetylated tubulin (Sigma-Aldrich; diluted 1:500). After washes in PBTr (PBS, 0.8% Triton X-100), larvae were incubated for 72 hours at 4 °C with the secondary antibody AlexaFluor 594 goat anti-mouse (1:400, Invitrogen).

For glia immunostaining, larvae were anesthetized in MS222 and fixed in 4% PFA, overnight at 4 °C. After several washes in PBS, they were incubated overnight at 4 °C in 20% sucrose. Zebrafish were embedded in killik (OTC compound, 05-9801 BioOptica), and once frozen, the molds were cut at a cryostat (OTF5000, BioOptica) producing sections of 30 μm in thickness. The slices were quenched in glycine (0.1 M in PBS) for 10 minutes. After washes, the modified IB solution containing (%) 10 NGS, 5 BSA, 1 DMSO was applied for 1 hour at RT. Next, slices were incubated overnight at 4 °C with primary antibody against the GFAP (mouse, 1:400, Sigma-Aldrich). The day after, samples were washed in PBS and incubated for 4 hours at 4 °C with secondary anti-mouse 488 antibodies (1:400, Thermofisher).

Samples were mounted in Fluoromount-G (Invitrogen), and the images were acquired at the level of the 8th–13th somites using the confocal microscope Nikon A1R with the 488 and 594 solid-state laser. The images for the acetylated tubulin were acquired at the 40× (0.95 NA) objective using 0.5 μm steps through the entire larvae thickness, while the GFAP images were acquire at the 100× (1.45 NA) oil objective, using 0.5 μm steps for the total thickness of the spinal cord at the level of 8th–10th somites. The number of branches in spinal ventral roots formed by motoneuron axons was manually counted using Fiji software, whereas GFAP volumetric analysis was performed thanks to Volocity (USA) software.

5.14 Statistics

All the data sets of calcium imaging, immunofluorescence, survival and anatomical characterization experiments underwent to the analysis of distribution using the D'Agostino Pearson omnibus normality test. Data that did not follow a Gaussian distribution were analyzed using Kruskal–Wallis multiple comparison test (with Dunn's test as *post-hoc* test), while for those following a Gaussian distribution we used the Brown–Forsythe and Welch One-Way ANOVA test, with Dunnett's T3 as *post-hoc* test. Calcium imaging data for injections at 5 μg mL^{-1} of MoS_2 were analyzed using paired Mann–Whitney test.

Regarding the behavioral experiments, the data sets were analyzed using Two-Way ANOVA followed by Sidak multiple comparisons test. All the plots of the manuscript were expressed as Mean ± SEM and N = number of individuals, unless stated otherwise.

Differences were considered as statistically significant when: $*P < 0.05$, $**P < 0.01$ and $***P < 0.001$.

Conflicts of interest

There are no conflicts of interest to declare.

Acknowledgements

This work received funding from the European Union Horizon 2020 Research and Innovation Programme under grant agreement no. GrapheneCore3 (881603). This study forms part of the Advanced Materials programme and was supported by MCIN with funding from European Union NextGenerationEU (PRTR-C17.I1), Junta de Comunidades de Castilla-La Mancha and project PID2020-113080RB-I00.

References

1 M. Samadi, N. Sarikhani, M. Zirak, H. Zhang, H.-L. Zhang and A. Z. Moshfegh, *Nanoscale Horiz.*, 2018, **3**, 90–204.

2 W. Wu, L. Wang, Y. Li, F. Zhang, L. Lin, S. Niu, D. Chenet, X. Zhang, Y. Hao, T. F. Heinz, J. Hone and Z. L. Wang, *Nature*, 2014, **514**, 470–474.

3 K. F. Mak and J. Shan, *Nat. Photonics*, 2016, **10**, 216–226.

4 X. Zhou, H. Sun and X. Bai, *Front. Bioeng. Biotechnol.*, 2020, **8**, 236.

5 S. Manzeli, D. Ovchinnikov, D. Pasquier, O. V. Yazyev and A. Kis, *Nat. Rev. Mater.*, 2017, **2**, 1–15.

6 Z. Xu, J. Lu, X. Zheng, B. Chen, Y. Luo, M. N. Tahir, B. Huang, X. Xia and X. Pan, *J. Hazard. Mater.*, 2020, **399**, 123057.

7 T.-W. Lee, Y.-H. Lai, J.-L. Chen and C. Chen, *J. Environ. Manage.*, 2022, **324**, 116278.

8 V. Yadav, S. Roy, P. Singh, Z. Khan and A. Jaiswal, *Small*, 2019, **15**, e1803706.

9 C. Moore, D. Movia, R. J. Smith, D. Hanlon, F. Lebre, E. C. Lavelle, H. J. Byrne, J. N. Coleman, Y. Volkov and J. McIntyre, *2D Mater.*, 2017, **4**, 025065.

10 R. Wu, M. Dong and L. Lius, *Coatings*, 2023, **13**, 1122.

11 S. Roy, K. A. Deo, K. A. Singh, H. P. Lee, A. Jaiswal and A. K. Gaharwar, *Adv. Drug Delivery Rev.*, 2022, **187**, 114361.

12 E. E. Patton, L. I. Zon and D. M. Langenau, *Nat. Rev. Drug Discovery*, 2021, **20**, 611–628.

13 G. Bruni, P. Lakhani and D. Kokel, *Front. Pharmacol.*, 2014, **5**, 153.

14 D. Kokel and R. T. Peterson, *Briefings Funct. Genomics Proteomics*, 2008, **7**, 483–490.

15 E. Haque and A. C. Ward, *Nanomaterials*, 2018, **8**, 561.

16 H.-R. Jia, Y.-X. Zhu, Q.-Y. Duan, Z. Chen and F.-G. Wu, *J. Controlled Release*, 2019, **311–312**, 301–318.

17 G. Di Mauro, R. Rauti, R. Casani, G. Chimowa, A. M. Galibert, E. Flahaut, G. Cellot and L. Ballerini, *Nanomaterials*, 2021, **11**, 9.

18 S. Deng, E. Zhang, J. Tao, Y. Zhao, W. Huo, H. Guo, B. Zheng, X. Mu, K. Yuan, X. Deng, H. Shen, H. Rong, Y. Ma and W. Bian, *Toxicology*, 2023, **487**, 153462.

19 C. Ren, X. Hu, X. Li and Q. Zhou, *Biomaterials*, 2016, **93**, 83–94.

20 Y. Zhao, Q. Yang, D. Liu, T. Liu and L. Xing, *Ecotoxicol. Environ. Saf.*, 2022, **242**, 113896.

21 M. d'Amora and S. Giordani, *Front. Neurosci.*, 2018, **12**, 976.

22 G. Cellot, S. Vranic, Y. Shin, R. Worsley, A. F. Rodrigues, C. Bussy, C. Casiraghi, K. Kostarelos and J. R. McDearmid, *Nanoscale Horiz.*, 2020, **5**, 1250–1263.

23 Y. Roussel, S. F. Gaudreau, E. R. Kacer, M. Sengupta and T. V. Bui, *eLife*, 2021, **10**, e67453.

24 V. J. González, A. M. Rodríguez, I. Payo and E. Vázquez, *Nanoscale Horiz.*, 2020, **5**, 331–335.

25 R. Shahzad, T. Kim and S.-W. Kang, *Thin Solid Films*, 2017, **641**, 79–86.

26 M. Cao, R. Cai, L. Zhao, M. Guo, L. Wang, Y. Wang, L. Zhang, X. Wang, H. Yao, C. Xie, Y. Cong, Y. Guan, X. Tao, Y. Wang, S. Xu, Y. Liu, Y. Zhao and C. Chen, *Nat. Nanotechnol.*, 2021, **16**, 708–716.

27 Z. Yang and K. K. W. Wang, *Trends Neurosci.*, 2015, **38**, 364–374.

28 V. Giacco, G. Panattoni, M. Medelin, E. Bonechi, A. Aldinucci, C. Ballerini and L. Ballerini, *J. Neuroinflammation*, 2019, **16**, 127.

29 G. Panattoni, R. Amoriello, C. Memo, A. Thalhammer, C. Ballerini and L. Ballerini, *Mol. Brain*, 2021, **14**, 159.

30 G. Di Mauro, R. Amoriello, N. Lozano, A. Carnasciali, D. Guasti, M. Becucci, G. Cellot, K. Kostarelos, C. Ballerini and L. Ballerinis, *ACS Nano*, 2023, **17**, 1965–1978.

31 E. Brustein, N. Marandi, Y. Kovalchuk, P. Drapeau and A. Konnerth, *Pflugers Arch.*, 2003, **446**, 766–773.

32 E. M. Hol and M. Pekny, *Curr. Opin. Cell Biol.*, 2015, **32**, 121–130.

33 M. Medelin, V. Giacco, A. Aldinucci, G. Castronovo, E. Bonechi, A. Sibilla, M. Tanturli, M. Torcia, L. Ballerini, F. Cozzolino and C. Ballerini, *Mol. Brain*, 2018, **11**, 3.

34 M. J. O'Donovan, A. Bonnot, P. Wenner and G. Z. Mentis, *Cell Calcium*, 2005, **37**, 443–450.

35 Y. Momose-Sato and K. Sato, *Front. Cell. Neurosci.*, 2013, **7**, 36.

36 K. J. Turner, T. G. Bracewell and T. A. Hawkins, *Methods Mol. Biol.*, 2014, **1082**, 197–214.

37 W. Zhang, D. Xiao, Q. Mao and H. Xia, *Signal Transduction Targeted Ther.*, 2023, **8**, 267.

38 Y. Chen, X. Hu, J. Sun and Q. Zhou, *Nanotoxicology*, 2016, **10**, 42–52.

39 X. T. Liu, X. Y. Mu, X. L. Wu, L. X. Meng, W. B. Guan, Y. Q. Ma, H. Sun, C. J. Wang and X. F. Li, *Biomed. Environ. Sci.*, 2014, **27**, 676–683.

40 D. G. Heijerick and S. Carey, *Sci. Total Environ.*, 2017, **609**, 420–428.

41 G. Peng and B. Fadeel, *Adv. Drug Delivery Rev.*, 2022, **188**, 114422.

42 C. H. Lee and P. C. Ruben, *Channels*, 2008, **2**, 407–412.

43 A. Verkhratsky, *Acta Pharmacol. Sin.*, 2006, **27**, 773–780.

44 T. Wyss-Coray and L. Mucke, *Neuron*, 2002, **35**, 419–432.

45 D. Kempuraj, R. Thangavel, P. A. Natteru, G. P. Selvakumar, D. Saeed, H. Zahoor, S. Zaheer, S. S. Iyer and A. Zaheer, *J. Neurosurg. Spine*, 2016, **1**, 1003.

46 C. Larrucea, P. Castro, F. J. Sepulveda, G. Wandersleben, J. Roa and L. G. Aguayo, *Brain Res.*, 2008, **1218**, 70–76.

47 A. Gorij, *Int. J. Mol. Sci.*, 2022, **23**, 5744.

48 J. R. Fetcho, S.-I. Higashijima and D. L. McLean, *Brain Res. Rev.*, 2008, **57**, 86–93.

49 L. J. Neukomm and M. R. Freeman, *Trends Cell Biol.*, 2014, **24**, 515–523.

50 Y. Yu, Y. Yi, Y. Li, T. Peng, S. Lao, J. Zhang, S. Liang, Y. Xiong, S. Shao, N. Wu, Y. Zhao and H. Huang, *RSC Adv.*, 2018, **8**, 17826–17836.

51 J. Rességuier, E. Delaune, A.-L. Coolen, J.-P. Levraud, P. Boudinot, D. Le Guellec and B. Verrier, *Front. Immunol.*, 2017, **8**, 190.

52 U. Strähle, S. Scholz, R. Geisler, P. Greiner, H. Hollert, S. Rastegar, A. Schumacher, I. Selderslaghs, C. Weiss, H. Witters and T. Braunbeck, *Reprod. Toxicol.*, 2012, **33**, 128–132.

53 D.-H. Pham, B. De Roo, X.-B. Nguyen, M. Vervaele, A. Kecskés, A. Ny, D. Copmans, H. Vriens, J.-P. Locquet, P. Hoet and P. A. M. de Witte, *Sci. Rep.*, 2016, **6**, 37145.

54 M. R. Miller, J. B. Raftis, J. P. Langrish, S. G. McLean, P. Samutrtai, S. P. Connell, S. Wilson, A. T. Vesey,

P. H. B. Fokkens, A. J. F. Boere, P. Krystek, C. J. Campbell, P. W. F. Hadoke, K. Donaldson, F. R. Cassee, D. E. Newby, R. Duffin and N. L. Mills, *ACS Nano*, 2017, **11**, 4542–4552.

55 K. Li, Z. Wang, H. Zeng, J. Sun, Y. Wang, Q. Zhou and X. Hu, *Nanotoxicology*, 2021, **15**, 114–130.

56 H. Lin, A. E. del Rio Castillo, V. J. González, L. Jacquemin, J. K. Panda, F. Bonaccorso, E. Vázquez and A. Bianco, *NanoImpact*, 2023, **29**, 100451.

57 I. Janica, D. Iglesias, S. Ippolito, A. Ciesielski and P. Samorı, *Chem. Commun.*, 2020, **56**, 15573.

58 R. Rauti, N. Lozano, V. León, D. Scaini, M. Musto, I. Rago, F. P. Ulloa Severino, A. Fabbro, L. Casalis, E. Vázquez, K. Kostarelos, M. Prato and L. Ballerini, *ACS Nano*, 2016, **10**, 4459–4471.

59 A. Franceschi Biagioni, G. Cellot, E. Pati, N. Lozano, B. Ballesteros, R. Casani, N. C. Coimbra, K. Kostarelos and L. Ballerini, *Biomaterials*, 2021, **271**, 120749.

60 R. M. Basnet, D. Zizioli, S. Taweedet, D. Finazzi and M. Memo, *Biomedicines*, 2019, **7**, 23.

61 K. M. Carter, C. M. Woodley and R. S. Brown, *Rev. Fish Biol. Fish.*, 2011, **21**, 51–59.

62 D. M. Parichy, M. R. Elizondo, M. G. Mills, T. N. Gordon and R. E. Engeszer, *Dev. Dyn.*, 2009, **238**, 2975–3015.

63 J. Karlsson, J. von Hofsten and P. E. Olsson, *Mar. Biotechnol.*, 2001, **3**, 522–527.